MECTA: MEMORY-ECONOMIC CONTINUAL TEST-TIME MODEL ADAPTATION

Junyuan Hong[1,*], **Lingjuan Lyu**[2], **Jiayu Zhou**[1], **Michael Spranger**[2]
[1]Michigan State University, [2]Sony AI
{hongju12,jiayuz}@msu.edu, {lingjuan.lv,michael.spranger}@sony.com

ABSTRACT

Continual Test-time Adaptation (CTA) is a promising art to secure accuracy gains in continually-changing environments. The state-of-the-art adaptations improve out-of-distribution model accuracy via computation-efficient online test-time gradient descents but meanwhile cost about times of memory versus the inference, even if only a small portion of parameters are updated. Such high memory consumption of CTA substantially impedes wide applications of advanced CTA on memory-constrained devices. In this paper, we provide a novel solution, dubbed MECTA, to drastically improve the memory efficiency of gradient-based CTA. Our profiling shows that the major memory overhead comes from the intermediate cache for back-propagation, which scales by the batch size, channel, and layer number. Therefore, we propose to reduce batch sizes, adopt an adaptive normalization layer to maintain stable and accurate predictions, and stop the back-propagation caching heuristically. On the other hand, we prune the networks to reduce the computation and memory overheads in optimization and recover the parameters afterward to avoid forgetting. The proposed MECTA is efficient and can be seamlessly plugged into state-of-the-art CTA algorithms at negligible overhead on computation and memory. On three datasets, CIFAR10, CIFAR100, and ImageNet, MECTA improves the accuracy by at least 8.5% with constrained memory and significantly reduces the memory costs of ResNet50 on ImageNet by at least 70% without sacrificing accuracy. Our codes can be accessed at https://github.com/SonyAI/MECTA.

1 INTRODUCTION

Many machine-learning applications require deploying well-trained deep neural networks from a large dataset to out-of-distribution (OOD) data and dynamically-changing environments, for example, unseen data variations (Dong et al., 2022; Liu et al., 2023) or corruptions caused by weather changes (Hendrycks & Dietterich, 2019; Koh et al., 2021). Hence, the recent efforts aim to tackle this emerging research challenge via continual test-time adaptation (CTA). The unsupervised, resource-constrained, and dynamic test-time environments in CTA make it a challenging learning problem and call for a self-supervised, efficient and stable solution. Decent examples include Tent (Wang et al., 2021) and EATA (Niu et al., 2022). Early in 2017, Li et al. found that updating batch-normalization (BN) layers with all test-time data without any training greatly improved the model OOD performance. Recently, Tent (Wang et al., 2021) significantly improved the test-time performance by minimizing the prediction entropy in an efficient manner where only a few parameters are updated. More recently, EATA (Niu et al., 2022) improved sample efficiency and evade catastrophic forgetting of the in-distribution data.

While Tent and EATA had achieved impressive gains on OOD accuracy via online optimization, such optimizations are accompanied by large memory consumption and are prohibitive in many real-world CTA applications. Since many devices are only designed for on-device inference rather than training, memory-limited devices, like small sensors, cannot afford CTA algorithms. In Fig. 1, we demonstrate that Tent/EATA adaptation of ResNet50 (He et al., 2016) with a batch size of 64 (the default setting in Tent) costs more than 5 times of memory in `model.backward` as the standard inference on ImageNet-C (Hendrycks & Dietterich, 2019). The large peak memory consumption makes EATA or

*Work was done during the internship at Sony AI. Correspondence to Lingjuan Lyu

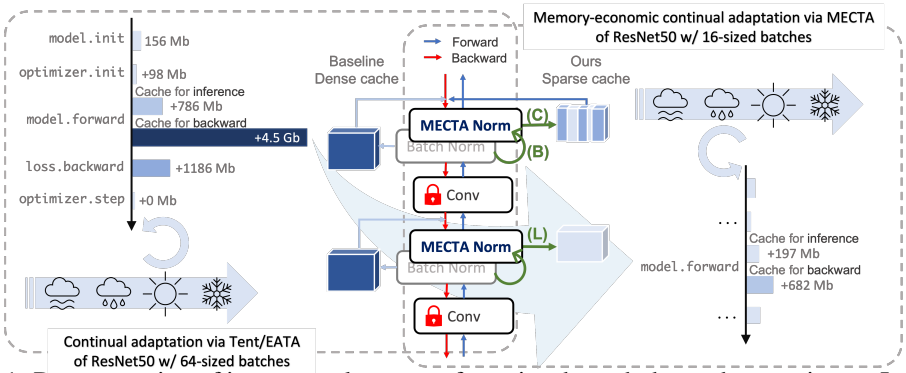

Figure 1: Demonstration of incremental memory footprints brought by each operation on ImageNet and illustration of the proposed MECTA method, which reduces the cache size of gradient-based adaptation. During forwarding, the MECTA Norm **(B)** stabilizes the normalization-statistic estimation via shift-aware moving-average from *small batches*, **(C)** randomly drops caches by *channel* admitting sparse gradient descent without knowing gradient in advance, and **(L)** maintains caches only for *layers* on demand of training.

Tent impossible to be adopted on edge devices, for example, the popular board-computer, Raspberry Pi with 1 Gb RAM, and old-generation of smartphones (Ignatov et al., 2018).

Observing the bottleneck on `model.backward`, a straightforward solution could be reducing batch sizes and model scales (including the number of channels and layers), but there are several obstacles to maintaining model performance simultaneously. First, a large batch size is essential for adaptation (Yang et al., 2022). Second, the amount of information extracted by a deep and wide model is desired for modeling distributionally-robust semantic features (Hendrycks et al., 2020a).

In this paper, we tackle the aforementioned challenges by proposing a novel approach called Memory-Economic Continual Test-time Adaptation (MECTA). As illustrated in Fig. 1, our method is enclosed into a simple normalization layer, MECTA Norm, to reduce the three dimensions of intermediate caches: batch, channel and layer sizes. (**B**) MECTA Norm accumulates distribution knowledge from streaming mini-batches and is stable on small batches and on shifts between domains using a shift-aware forget gate. (**C**) Resembling sparse-gradient descents, we introduce test-time pruning that stochastically removes channels of cached intermediate results without knowing gradient magnitudes. (**L**) The forget gate also guides the layer adaptation: if the layer distribution gap is sufficiently small, then the layer will be excluded from memory-intensive training. Our contributions are as follows.

• *New Problem*: We initiate the study on the memory efficiency of continual test-time adaptation, revealing the substantial obstacle in practice.

• *New Method*: We propose a novel method that improves the memory efficiency of different CTA methods. The simple norm layer structure is ready to be plugged into various networks to replace batch-normalization. The MECTA Norm layer also enables us to stop and restart model adaptation without unused or absent caches for unwanted or on-demand back-propagation. Without forgetting due to removing parameters, our pruning is conducted on cache data for back-propagation rather than forwarding and can greatly reduce memory consumption.

• *Compelling Results*: Our method maintains comparable performance to full back-propagation methods while significantly reducing the dynamic and maximal cache overheads. Given limited memory constraints, our method improves the Tent and EATA by $8.5 - 73\%$ accuracy on CIFAR10-C, CIFAR100-C, and ImageNet-C datasets.

2 Related Works

Test-time Adaptation (TTA) aims to improve model accuracy on Out-of-Distribution (OOD) data by adapting models using unlabeled test data. In comparison, traditional learning algorithms train models robustly, e.g., distributionally robust neural networks (Sagawa et al., 2020) or adversarial training (Deng et al., 2023), in order to generalize to OOD data. Early examples for TTA include the test-time training (TTT) (Sun et al., 2020) and its variant (Liu et al., 2021) which jointly train a source model via both supervised and self-supervised objectives, and then adapt the model via self-supervised objectives at test time. Adaptive risk minimization (Zhang et al., 2021), contextual

meta-learning, conditional neural process (Garnelo et al., 2018) train models that can be adapted using inferred context information from test data. Though plausible, these methods are in need of a redesign of the training process. Thus, they are less applicable for many off-the-shelf models pre-trained on datasets that are too big to attain by a small device or are prohibited from unauthorized sharing. To address the problem, training-agnostic adaptation methods are proposed recently, through adapting batch-normalization statistics (Nado et al., 2021; Schneider et al., 2020; Khurana et al., 2022), minimizing unsupervised entropy losses (Wang et al., 2021; Goyal et al., 2022), maximizing prediction consistency over multiple augmentations (Zhang et al., 2022), and classifier adjustment (Iwasawa & Matsuo, 2021). Though these methods are effective, their applicability is limited to a constant test environment in contrast real scenarios.

Efficient Continual Test-time Adaptation (CTA) considers the test scenario with dynamically changing rather than static environments and calls for efficient adaptation in place and in time. Wang et al. initiated the continual setting on computer vision by augmented supervision, which however has a large computation hurdle due to multiple times of inference on one sample. The BN-based approaches are efficient alternatives, which only need to update statistics (Nado et al., 2021; Schneider et al., 2020). Yet, it has been shown in recent research that removing covariate shift by BN is not enough for reaching the supervised performance (Wang et al., 2021; Niu et al., 2022). In comparison, Tent is more effective and efficient with one-time back-propagation per sample (Wang et al., 2021). Later, Niu et al. (2022) improved the sample efficiency via selective back-propagation. Despite the advance of CTA in computation efficiency, the memory efficiency is overlooked regardless its importance in on-device adaptation. Plausible directions are on-device sparse (continual) learning (Wang et al., 2022b; Mallya et al., 2018; Mallya & Lazebnik, 2018) or fine-tuning (Jiang et al., 2022; Cai et al., 2020), but how to conduct memory-efficient learning without labels is still unclear. In this paper, we inspect the gradient computation in parameter-efficient adaptation and disclose the main bottleneck for striking the balance between memory consumption of feature caches and learning effectiveness. Based on the analysis, we propose a novel solution to reduce caches by batch, channel and layer reductions without sacrificing performance.

3 Problem Formulation

Let $P(x)$ denote the data distribution sampled from the set of distributions $\mathcal{P}$, and P_0 is the training distribution. We assume that a distributions in $P \sim \mathcal{P}$ is either identical to or is biased from P_0 a lot. A neural network model f_θ parameterized by θ is pre-trained on the training set P_0 by $\theta_0 = \min_{\theta\in\Theta} \mathbb{E}_{x\sim P_0(x)}[\ell(f_\theta(x), c(x))]$, where $c(x)$ is an oracle function for ground-truth labels and ℓ is a loss function defined over the sample x and model parameter θ. One example of the loss is the cross-entropy loss: $\ell_{\text{ent}}(f_\theta(x), c(x)) = -\sum_i c(x)_i \log f_\theta(x)_i + \log \sum_i \exp f_\theta(x)_i$ given logits from a θ-governed model $f_\theta(x)$. With the pre-trained model, Tent and EATA continually adapt the model via recursive updating,

$$\theta_t = \text{Optimize}_{\theta\in\Theta_t}(\mathbb{E}_{x\sim P_t(x)}[H(f_\theta(x))], \theta_{t-1}),\ P_t \sim \mathcal{P}, \tag{1}$$

for step $t \in \{1, 2, 3, \dots\}$, where $\text{Optimize}(\cdot,\cdot)$ represents a generic optimization algorithm minimizing the first variable given θ initialized by θ_{t-1}. Without labels, the entropy function $H(f_\theta(x)) = \ell_{\text{ent}}(f_\theta(x), f_\theta(x))$ resembles the cross-entropy loss with self-supervisions in Tent.

Parameter-efficient adaptation. As the efficiency is critical at test-time, we focus on the state-of-the-art efficient solution to the CTA: EATA and Tent, both of which adopt the one-step gradient descent as the optimization strategy in Eq. (1). Thus, $\text{Optimize}_{\theta\in\Theta_t}(\mathbb{E}H, \theta_{t-1}) = \theta_{t-1} - \eta \frac{\partial}{\partial\theta}\mathbb{E}H$ given a learning rate η. To efficiently train models, we constrain the parameter space in a subspace of the original one, denoted as $\Theta_t = \tilde{\Theta} \subset \Theta$. We follow Tent and EATA to make the parameters trainable in the batch-normalization layers (BN layer).

Now, we give a brief introduction to the batch-normalization layer (Ioffe & Szegedy, 2015). Let the input to the layer l be a *batch* of features denoted as x^l in the real space of dimension $B \times C^l \times H^l \times W^l$, where B is the batch size, C^l is the number of channels, H^l and W^l are the height and width. We use $[N]$ to denote the set $\{1, \cdots, N\}$. For $(n, i, j, k) \in [B]\times[C^l]\times[H^l]\times[W^l]$ and small constant ϵ_0, the BN layer is defined as two sequential channel-wise operations,

$$z^l_{n,i,j,k} = \frac{x^l_{n,i,j,k} - \mu^l_i}{\sqrt{\sigma^2_i + \epsilon_0}} \text{ (normalization)},\ a^l_{n,i,j,k} = \gamma^l_i z^l_{n,i,j,k} + b^l_i \text{ (affine)}, \tag{2}$$

where $\mu_i^l, {\sigma_i^l}^2$ are the mean and variance of x^l in channel i, respectively. The output tensor a is also called activation. For Tent and EATA, only the affine parameters, γ and b, are trainable.

4 Proposed Method

In this section, we elaborate on the proposed method that improves the memory efficiency of gradient-based adaptation methods. First, straightforward derivations show that the intermediate representations ought to be stored for computing the gradients of affine layers and therefore forge a huge memory overhead. Suppose the loss on the n-th sample is ℓ_n. Based on Eq. (2), the gradient w.r.t. the i-th channel affine weight γ_i is

$$\sum_{n=1}^{B} \frac{\partial \ell_n}{\partial \gamma_i^l} = \sum_{n=1}^{B} \sum_{j=1}^{W} \sum_{k=1}^{H} \frac{\partial \ell_n}{\partial a_{i,j,k}^l} z_{n,i,j,k}^l. \tag{3}$$

Therefore, to compute the gradient, each BN layer has to store the normalized representations z^l (*cache*) of the dimension $B \times C^l \times W^l \times H^l$ at forwarding until $\partial \ell_n / \partial a_{i,j,k}^l$ is available. For an L-layer network, the inference-only memory consumption of affine layers is $R_{\text{fwd}} = \max_{l \in \{1, \cdots, L\}} B \times C^l \times W^l \times H^l$. In comparison, the corresponding intermediate memory for back-propagation is accumulated by $R_{\text{bwd}} = \sum_{l=1}^{L} B \times C^l \times W^l \times H^l \geq R_{\text{fwd}}$. To reduce the memory overhead, a straightforward idea is to reduce B, C^l, and L by dropping corresponding entries in $\{z^l\}_{l=1}^L$, respectively. Since dropping entries in $\{z^l\}_{l=1}^L$ will vanish the corresponding gradients, the strategy will easily break down the learning if not carefully handled. Below, we will discuss the obstacles and our solutions for accuracy-secured cache reduction by B, C^l, and L dimensions, respectively.

(Reduce B) Adaptive statistic estimation on dynamic distributions. As a sufficient number of samples are essential for accurate statistic estimation (μ and σ^2) per BN layer, reducing samples in a batch will bias the statistics for normalization. In standard or test-time training, exponential moving average (EMA) has been widely used to mitigate the bias by memorizing streamed batches (Yang et al., 2022; Chiley et al., 2019; Liao et al., 2016). To preserves the property of gradient on calibrated statistics, we follow Yang et al. and Schneider et al. to implement the EMA normalization at test time. Let ϕ be the composed tuple, $[\mu, \sigma]$, for mean and variance in a BN layer. ϕ_t denotes the running statistics at iteration t and $\hat{\phi}_t$ is the one from the t-th batch. The EMA statistics are

$$\phi_t = (1 - \beta)\phi_{t-1} + \beta \hat{\phi}_t, \tag{4}$$

where the parameter $\beta \in [0, 1]$ governs the memory length and therefore works as the *forget gate*. A small β endorses the model with long-term memory, otherwise short-term memory.

Traditionally, β is constant at running time, which however cannot accommodate the estimation to the *dynamic* distributions P_t. Intuitively, when a model is stably running in a single domain, e.g., $P_t \approx P_t$, β should be small to keep as many data points as possible to support accurate statistic estimation. In contrast, when the distribution is shifting, e.g., $P_t \neq P_{t-1}$, β should be large for avoiding the mixture of two distinct statistics. Complying with the intuition, we introduce a forgetting gate to calibrate the β adaptively, $\beta_t = h(\phi_{t-1}, \hat{\phi}_t)$, where $h(\cdot, \cdot)$ captures the distributional shifts. We consider a non-parametric heuristic definition of $h(\cdot, \cdot)$ as follows.

$$\beta_t = 1 - e^{-D(\phi_{t-1}, \hat{\phi}_t)}, \; D(\phi_{t-1}, \hat{\phi}_t) = \tfrac{1}{C} \sum\nolimits_{i=1}^{C} KL(\phi_{t-1,i} \| \hat{\phi}_{t,i}) + KL(\hat{\phi}_{t,i} \| \phi_{t-1,i}), \tag{5}$$

where $D(\cdot, \cdot)$ is a properly-defined distance function measuring distribution shifts. The KL divergence, $KL(\phi_1^i \| \phi_2^i)$, is defined as $\log \sigma_2^i - \log \sigma_1^i + \frac{1}{2{\sigma_2^i}^2}({\sigma_1^i}^2 + (\mu_1 - \mu_2)^2) - \frac{1}{2}$ assuming two Gaussian distributions parameterized by ϕ_1 and ϕ_2, respectively. The distance function is inspired by Li et al. (2017), where the authors showed that ϕ_1 and ϕ_2 have larger KL divergence (based on a Gaussian assumption) if they are from distinct domains. In addition, β_t^l is estimated layer by layer, as the distribution of different layers will shift to different degrees. Intuitively, when the $(l-1)$-th layers are well aligned after calibrating ϕ_t^l, the deep layers should be aligned better.

(Reduce C) Sparse gradients via stochastically-pruned caches. It is easy to see that dropping the caches the channel i in z will vanish the corresponding gradient at the channel and may leave

the corresponding affine parameter underfitted. Thus, trivially pruning channels would cast serious issues, especially when some channels are critical for OOD generalization (Sehwag et al., 2020). But, it is hard to predict which gradient is such important not to be pruned before it is computed. Therefore an efficient pruning strategy without depending on back-propagation is desired. For this purpose, we propose an unconditioned pruning strategy by repeatedly generating a stochastic mask M *per iteration* such that $q \times 100\%$ entries of the mask are zeros and the rest are ones. Given the input tensor z to the affine layer, we mask the tensor by $\tilde{z}_{n,i,j,k} = M_i z_{n,i,j,k}$ for caches in Eq. (3).

Our pruning strategy has multi-fold merits. Since forwarding is not influenced, the prediction can be done still on the full size of the network preserving a high quality of semantic features. Meanwhile, pruning lowers memory usage significantly with much smaller intermediate caches and gradients. The recomputed masks per iteration resembles a progressive learning paradigm and the momentum technique in modern optimizers, like SGD or Adam, can impute the missing gradients. Moreover, the approach mitigates catastrophic forgetting since only a subset of affine weights are updated and the low-magnitude parameters are not updated. Specifically, given gradients g_t, the model difference $\|\theta_t - \theta_0\| = \|\sum_t g_t\| \leq \mathcal{O}(\sum_t \|g_t\|)$ will be reduced with some zeroed $\|g_t\|$, which can be viewed as an implicit anti-forgetting regularization in EATA. Later, we empirically demonstrate the regularization effect in mitigating the forgetting in regularization-free Tent.

(Dynamic L) Train layers on demand. Most test-time adaptations will last for a long time in a single environment. For example, an auto-driving car will keep running in sunny weather for long daytime, producing thousands of images. Continually adapting the model to the same environment for an overly-long time will not improve models continually but waste resources. Thus, we propose to stop the back-propagation if the optimization converges and we restart it on demand of adaptation. The principle is that *the adaptation is demanded when data distribution fundamentally shifts.* Recalling that we already measure the distributional shift by Eq. (5), we reuse the metric to guide the adaptation. Specifically, we use a threshold β_{th} to make the decision. If $\beta_t^l \leq \theta_{\text{th}}$, then the z^l is cached for back-propagation. Because of the layer-wise decision, any layer can halt training to save a lot of memory early before the network is fully executed or the optimization of all layers converge. This technique can introduce dynamic memory allocation, benefiting multi-task mobile systems. For example, the extra memory freed by the training can be used for other apps on the smartphone.

Finally, we summarize the proposed method in Algorithm 1, where our method includes three hyper-parameters to trade off accuracy and memory. Notably, our method is fully enclosed in a MECTA Norm layer, which can be easily embedded into a network, like the widely-used ResNet (He et al., 2016), to enhance the memory efficiency at test-time adaptation.

Algorithm 1 Memory-Economic Continual Test-time Adaptation (MECTA)

Input: A model f_θ with L MECTA Norm layers, the total number of iterations T, pruning rate q, batch size B and layer cache threshold β_{th}.

for iteration $t \in \{1, \cdots, T\}$ **do**
  Initiate intermediate cache: $Z = \emptyset$
  for MECTA Norm layer $l \in 1, \ldots, L$ **do**
    Get layer input x^l;
    Compute the current batch statistics $\hat{\phi}_t^l$;
    Compute forget gate β_t^l by Eq. (5) and the statistics ϕ_t^l by Eq. (4); ▷ Stable statistics with reduced B
    Compute a_t^l and z^l by Eq. (2) using ϕ_t^l;
    if $\beta_t^l > \beta_{\text{th}}$ **then** ▷ Dynamic L
      Randomly remove $q \times 100\%$ of channels in z_t^l and cache $Z = Z \cup \{z_t^l\}$; ▷ Reduce C
    Output a^l to the next layer;
  Compute loss and back-propagate gradients with cache Z to update parameters;

Critical difference to prior work on memory footprint reduction. Previous attempts to reduce footprint (Wang et al., 2022b; Yuan et al., 2021) focused on parameter sparsity and reduce the overhead of storing model parameters and gradients. However, the overhead of parameters or gradients is relatively small in comparison to the caches for backwarding, as shown in Fig. 1. Instead, we focus on the large overheads of caches and our method is ready to work with the traditional parameter sparsity. For this purpose, our channel pruning and on-demand layer training resembles the gradient sparsity (Garg & Khandekar, 2009) or coordinate descent (Wright, 2015), and the two tactics implicitly prune the gradients before back-propagation avoiding large caches. Other than gradient

sparsity, gradient checkpointing (GC) Chen et al. (2016) is a more general way to reduce memory footprint. GC only caches the inputs of segments of layers and recompute intermediate features on demand. The optimal memory reduction is about the $1/\sqrt{L}$ of the original cost. Both GC and our method can greatly reduce the memory, but our method is favored because MECTA can reduce the memory on demand, MECTA is more computation efficient.

5 EXPERIMENTS

Datasets and pre-trained models. To evaluate the OOD generalization of models, we adopt three image-classification datasets: the CIFAR10-C, CIFAR100-C (Krizhevsky, 2009) and ImageNet-C (Deng et al., 2009) following previous arts (Niu et al., 2022). All the datasets are processed with 15 kinds of corruptions from 4 main categories (noise, blur, weather, and digital ones) with the highest severity level 5, which are widely used as the robustness benchmark for deep learning (Hendrycks & Dietterich, 2019). Without specifications, we use the ResNeXt29-32×4d pre-trained by AugMix (Hendrycks et al., 2020b) for CIFAR10-C and CIFAR100-C, and the ResNet50 pre-trained by Hendrycks et al. (2020a) for ImageNet-C, which has compelling robust performance in the benchmark learderboard (Croce et al., 2021).

Baselines. Our method is ready to replace batch-normalization in adaptable networks for better OOD generalization. **(1) CTA.** Therefore, we plug the proposed MECTA into two backbone methods: Efficient Anti-forgetting Test-time Adaptation (EATA) (Niu et al., 2022) and Test-time entropy minimization (Tent) (Sun et al., 2020). We also include the simplest BN statistic adaptation (BN) (Schneider et al., 2020) which is the most memory- and computation-efficient test-time adaptation only updating BN statistics without gradients. Tent improves the model accuracy via self-supervision and constrains the parameter updating to affine layers. EATA is the state-of-the-art efficient solution that balances computation efficiency and accuracy well. We plug MECTA into them to show the potential improvements in accuracy, efficiency, and generality on methods with advanced principles. Though other methods are also applicable to the problem, they typically lack advantages in efficiency, thus out of our scope. **(2) Memory reduction.** Gradient checkpointing (GC) Chen et al. (2016) is a general method for reducing memory costs in training, which trades in computation for memory and is applicable with any sequential structure. We apply GC to ResNet where we treat each block (including several conv-bn-relu layers) as the minimal unit and segment ResNet into $\sqrt{L}$ parts.

Evaluation setup. We conduct experiments on the *lifelong* setting, where the batches of data come in a streaming manner. For privacy considerations, no data shall be stored for memorization. Similarly, the types of corruption also arrive sequentially and are agnostic to the model. Thus, models have to be adapted online to gain higher accuracy on streaming data and environments. Such a setup can simulate a challenging yet realistic scenario, admitting high practical values.

Evaluation metrics. We adopt two metrics to evaluate the effectiveness and memory efficiency of different methods. (1) *Accuracy* (%) is evaluated on all samples under the same corruption with the highest level 5 by default. (2) *Cache size* (Mb). Since the memory of model parameters and optimizers is always constant or linearly dependent on the size of intermediate variables, we focus on the tensor size of intermediate variables. Specifically, we sum up the memory consumption of the tensor for affine layers, i.e. the *cache* z^l in Eq. (3). For the ease of memory accountant, we eclude other memory costs that are the same among different algorithms.

More details regarding hyper-parameters and implementation can be found in the appendix.

5.1 BENCHMARKS ON OOD PERFORMANCE

Comparison under the same cache constraint. We evaluate the accuracy with a constraint on the cache size. For this purpose, we let the gradient-free methods use a large batch size of 128 and a gradient-based method (Tent and EATA) select a small batch size from $\{4, 8, 16, 32\}$ such that the latter has a smaller maximal cache size than the former does. In Table 1, we report the per-domain accuracy in continual test-time adaptation in the column order, and we calculate the cache size on average and on maximum along the sequential adaptation. We have two main observations on MECTA. **(1) MECTA improves accuracy under cache constraints.** With the constraint, Tent and EATA have to adopt a small batch size and therefore perform poorly, even worse than gradient-free adaptation (BN). By reducing the cache dynamically, MECTA boosts the performance of EATA and Tent drastically by $8.5 - 73.0\%$ on all three datasets. EATA+MECTA shows the best performance in CIFAR10-C and ImageNet-C and comparable accuracy to Tent on CIFAR100-C. **(2) MECTA is more computation- and memory-efficient than GC.** Though GC lowers the memory costs,

it meanwhile increases the computation costs by around 20% in terms of GFLOPs. In contrast, our method only marginally increases the computation cost by less than 0.2% and can bear larger batches.

Table 1: Continual evaluation on three datasets regarding accuracy (%) and cache sizes (Mb). For a fair comparison, batch sizes (BS) are chosen such that the corresponding cache sizes are lower than those of BN with a batch size of 128. Orig. denotes the original data. Blue cells highlight the highest accuracy on the same dataset, and the bold texts indicate the best accuracy given the same base algorithm. GFLOPs is the number of 10^9 Floating Point Operations for adapting one sample. Results with more batch sizes are in Table 6.

		Noise			Blur				Weather				Digital					Acc.	Cache		GFLOPs
Alg.	BS	Gauss.	Shot.	Impul.	Defoc.	Glass.	Motion	Zoom.	Snow	Frost	Fog	Bright.	Contr.	Elast.	Pixel.	JPEG	Orig.	Avg	Avg	Max	
									CIFAR10-C												
BN	128	81.5	83.2	79.9	92.4	80.7	91.1	92.1	87.9	87.7	85.7	92.7	89.8	85.6	87.6	83.0	94.2	87.2	134	134	1.1
Tent	8	68.8	46.3	16.4	12.8	11.8	8.9	9.9	10.7	10.3	10.2	10.3	10.2	10.1	10.0	10.2	10.2	16.7	100	100	2.180
+GC	16	81.8	82.2	71.8	68.9	52.8	43.7	39.0	30.7	22.8	17.7	10.1	6.7	7.4	8.2	8.1	9.0	35.1	130	130	2.6
+MECTA	32	**87.0**	**88.6**	**85.7**	**91.8**	**84.5**	**90.9**	**92.5**	**90.1**	**91.3**	**88.8**	**93.2**	**92.0**	**88.0**	**90.5**	**86.0**	**93.8**	**89.7**	62	119	2.182
EATA	8	74.5	70.9	66.6	69.7	55.5	54.6	47.2	38.4	33.1	35.1	35.2	18.8	12.2	14.5	13.3	8.5	40.5	100	100	2.180
+GC	16	83.4	84.3	81.3	86.4	77.0	83.8	86.5	84.5	84.7	83.9	88.1	87.9	80.9	85.5	79.3	87.9	84.1	130	130	2.6
+MECTA	32	**87.1**	**89.3**	**86.8**	**92.0**	**85.6**	**90.7**	**92.3**	**90.8**	**91.1**	**89.7**	**93.3**	**92.5**	**88.0**	**91.0**	**86.9**	**93.5**	**90.0**	71	119	2.182
									CIFAR100-C												
BN	128	57.6	59.0	56.6	72.5	58.2	69.9	71.8	64.7	64.8	57.9	73.5	69.8	64.3	66.7	58.6	75.8	65.1	134	134	1.1
Tent	8	52.9	53.9	46.7	50.5	31.2	29.7	23.7	14.3	10.0	6.7	5.9	3.4	3.9	3.6	3.5	3.5	21.5	100	100	2.180
+GC	16	56.8	61.4	59.6	68.5	56.1	65.3	66.9	59.7	60.0	54.9	65.0	57.0	54.2	56.2	46.8	58.6	59.2	130	130	2.6
+MECTA	32	**58.6**	61.5	**60.1**	**73.9**	**61.0**	**72.4**	**74.9**	**66.8**	**68.1**	**61.9**	**75.3**	**71.3**	**66.7**	**70.5**	**61.7**	**78.1**	**67.7**	77	120	2.182
EATA	8	52.1	54.2	53.2	65.3	51.5	63.8	64.9	59.1	58.5	53.9	66.8	63.2	56.3	61.1	52.9	70.1	59.2	100	100	2.180
+GC	16	57.3	60.5	58.5	69.9	57.1	68.9	69.8	63.7	64.4	59.4	71.6	67.9	62.8	67.1	58.2	74.4	64.5	130	130	2.6
+MECTA	32	**58.7**	**62.0**	60.0	**73.0**	**60.5**	**71.3**	**73.9**	**66.7**	**67.3**	**62.0**	**75.3**	**71.7**	**66.3**	**69.8**	**61.5**	**78.0**	**67.4**	81	120	2.182
									ImageNet-C												
BN	128	39.2	42.6	39.6	29.9	32.9	40.8	47.4	45.0	47.7	55.8	68.5	36.0	54.8	65.4	55.7	74.2	48.5	411	411	4.1
TENT	8	33.8	16.5	0.8	0.4	0.3	0.4	0.4	0.4	0.4	0.3	0.4	0.2	0.3	0.4	0.3	0.4	3.5	307	307	8.183
+GC	16	43.3	46.1	42.8	25.8	14.8	5.0	1.3	0.7	0.7	0.7	0.8	0.6	0.7	0.7	0.7	0.7	11.6	404	404	10.3
+MECTA	32	**47.0**	**52.3**	**51.7**	**38.5**	**43.1**	**47.5**	**51.5**	**47.4**	**49.3**	**54.2**	**64.4**	**46.2**	**55.6**	**62.4**	**57.0**	**68.8**	**52.3**	269	373	8.190
EATA	8	34.1	37.0	35.0	27.5	28.1	35.5	38.6	39.6	39.7	47.8	56.6	35.5	44.1	53.3	46.7	63.2	41.4	307	307	8.183
+GC	16	44.4	47.1	45.4	39.0	39.4	47.4	49.7	49.7	48.4	57.6	64.3	47.8	54.5	61.7	56.3	69.5	51.4	404	404	10.3
+MECTA	32	**50.3**	**54.1**	**52.6**	**44.6**	**47.0**	**53.6**	**57.0**	**55.5**	**54.8**	**62.9**	**70.3**	**54.3**	**61.1**	**68.4**	**63.0**	**74.6**	**57.8**	288	373	8.190

Comparison using the same batch size. In Table 2, we follow the CTA protocol of (Niu et al., 2022) to compare the proposed method with other baselines, e.g., TTT (Sun et al., 2020), TTA (Ashukha et al., 2021), MEMO (Zhang et al., 2021) and CoTTA (Wang et al., 2022a). For a fair comparison, all methods only adapt BN layers if applicable, and use the standardly-trained ResNet50, which is publicly available, for example, from the official PyTorch package. **(1) MECTA is memory-efficient with the same batch size.** With only 30% of cache (or 70% of GC cache), MECTA maintains similar performance as the standard EATA. Notice that GC is less effective in cache reduction here than the reported results in (Chen et al., 2016), because the parameter-efficient adaption already drops a lot of caches for frozen convolutional layers. The cache cost of EATA+MECTA is pretty low which is only more than those of the BN and non-adapted source models, yet has a large gain (14.3%) on accuracy meanwhile. **(2) MECTA mitigates forgetting.** Note Tent has been known to suffer from catastrophic forgetting in continual adaptation (Niu et al., 2022) and thus has decreasing trend on the accuracy by sequential domains, and we find that our method can mitigate this issue. The inherent reason for the mitigation is quite intuitive: the MECTA will adaptively reduce the number of parameters to be updated, which is similar to the regularization of EATA on norm-bounded parameter distance. Also, we add the original dataset as the last domain in CTA to evaluate if the model forgets the original data. Both Tent and EATA have significantly lower accuracy on the original set with small batch size, while Tent/EATA+MECTA gains much higher original-set accuracy on all datasets, with an improvement of 7.6% at least (EATA on CIFAR100) and 69% at most (Tent on CIFAR10).

5.2 Qualitative Studies

In the following experiments, if not specified, we use ImageNet-C and robustly pre-trained ResNet50.

Effect of each component in ECTA on memory-accuracy trade-off. For brevity, we name the components as MECTA-X where X is **B** for adaptive forgetting, **C** for stochastic cache pruning and **L** for adaptive layer training. We define the accuracy averaged over all corruptions as the *mean-corruption acc*. An overall comparison with EATA and BN on mean-corruption acc is de-

Table 2: Comparison to other baselines with a batch size of 64 on the standardly-trained ResNet50 on ImageNet-C. #fwd and #bwd denote the times of forward and backward over a batch on average. GN is the group norm and JT denotes the model is jointly trained via supervised cross-entropy and rotation prediction losses. The bold numbers indicate the highest accuracy (or smallest cache) and the underlined ones are the second best result. Cache sizes with GC are in brackets.

	Noise			Blur				Weather				Digital				Acc.	Cache	#fwd	#bwd
Alg.	Gauss.	Shot.	Impul.	Defoc.	Glass.	Motion	Zoom.	Snow	Frost	Fog	Bright.	Contr.	Elast.	Pixel.	JPEG	Avg	Max (Mb)		
ResNet50; Reset model per perturbation																			
TTT (GN+JT)	31.0	33.6	33.4	28.1	7.8	33.2	36.8	40.9	19.0	51.0	61.8	38.9	49.4	51.7	48.0	37.6	2460×20	21	20
BN	15.5	16.1	16.3	20.0	20.0	28.5	40.0	34.8	35.0	48.5	65.9	24.1	45.8	50.7	41.1	33.5	**206**	1	0
TTA	4.1	4.9	4.5	12.5	8.2	12.9	25.8	14.0	19.1	21.3	53.0	12.4	14.6	24.6	33.6	17.7	**206**	64	0
MEMO	7.5	8.7	9.0	19.7	13.0	20.7	27.6	25.3	28.8	32.1	61.0	11.0	23.8	33.0	37.5	23.9	2460×65	65	65
ResNet50; Lifelong adaptation																			
CoTTA(+GC)	16.9	20.3	22.8	20.6	22.0	31.7	42.4	34.5	34.0	47.2	58.9	24.1	44.5	48.6	42.4	34.1	2460 (1618)	33	1
Tent(+GC)	28.4	34.1	31.7	19.3	12.2	6.9	4.0	1.4	0.8	0.7	0.9	0.4	0.6	0.7	0.6	9.5	2460 (1618)	1	1
Tent+MECTA	25.3	33.7	32.8	22.4	24.0	27.4	34.8	27.6	24.7	32.4	45.1	12.7	25.6	27.4	21.8	27.8	746	1	1
EATA(+GC)	**35.0**	38.1	36.8	**33.8**	34.2	**47.3**	**53.2**	**51.1**	**45.6**	**59.7**	**68.0**	**44.2**	**57.2**	**60.4**	54.7	**48.0**	2460 (1618)	1	**0.56**
EATA+MECTA	33.3	**40.1**	**39.2**	32.9	**35.0**	45.4	52.9	49.4	**45.6**	58.7	67.4	44.1	56.9	**60.4**	**55.5**	47.8	746	1	**0.56**

picted in Fig. 2a. For BN, we vary the batch size from {32, 64, 128, 256, 512}. For EATA and EATA+MECTA-B, we vary the batch size from {4, 8, 16, 32, 64} where 64 is the default setting from the original paper of EATA. For EATA+MECTA-BL, we let the batch size be 16 and vary the β_{th} in $\{1, 6.25, 12.5, 25, 50, 100, 200, 400\} \times 10^{-4}$. For EATA+MECTA-BLC, we let the batch size be 16 and β_{th} be 0.00125 and vary the pruning rate q in $\{0.1, 0.3, 0.5, 0.7, 0.9\}$.

The simplest BN method reaches the best accuracy at the batch size of 128 with approximately 400 Mb cache, which is much lower than the best accuracy achieved by EATA. However, given the same cache size, EATA does not perform better than BN. Only when 1200 Mb cache memory is occupied, EATA significantly outperforms BN by 5%. The need for a large batch (corresponding to a large cache) by EATA comes from the poor performance when the batch size is small, e.g., at a batch size of 8 or 16. MECTA-B treats EATA with a streaming normalization with adaptive forgetting and memorization leading to higher accuracy on small-batch adaptation. EATA+MECTA-B achieves better or comparable accuracy using either the smallest memory or the largest memory. Meanwhile, MECTA-L and MECTA-C improve the trade-off frontier into a low-cost zone. Given cache size lower than 600 Mb, MECTA-BL can beat the best accuracy of EATA. Last, with cache pruning, MECTA-BLC further improves the efficiency more impressively: best accuracy at an extremely small cache size (fewer than 100 Mb).

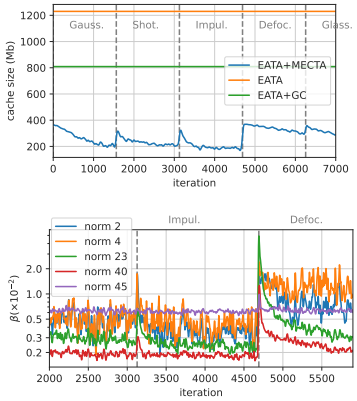

Figure 3: Dynamic cache sizes and layer-wise β using MECTA.

To understand the cache reduction, we study the memory/accuracy by three MECTA components.
(L) Adaptive layer-training. In Fig. 3, we show that the cache size will dynamically change by iterations using EATA+MECTA (batch size of 32). Especially, the cache size will peak at the beginning of distribution shifts and gradually vanishes. The β differs by layer and different layer has a different sensitivity to the distributional shifts, which motivate us to use set β and activate training layer-wisely. In Fig. 2b, when β_{th} is small, all layers will be trained and therefore the cache size is larger than the efficient BN adaptation. Increasing β_{th} reduces the cache size on average of the

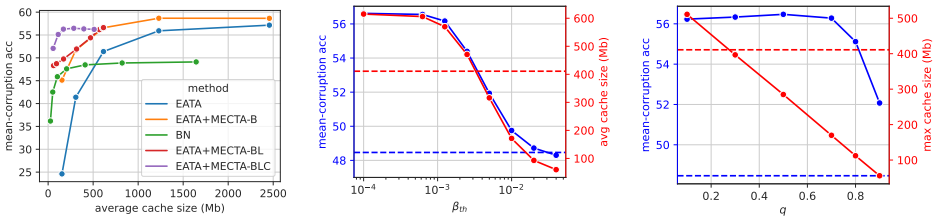

(a) Trade-off comparison. (b) Adaptive training (L). (c) Cache pruning (C).

Figure 2: Ablation study on the components of MECTA. The dash horizontal lines in (b) and (c) are the performance of BN with the best trade-off in (a) (of batch size 128).

Table 3: Ablation study of MECTA-B regarding accuracy (%) and a batch size of 16. Bold texts indicate the best accuracy among ablations. See Table 7 for other backbone methods.

	EMA	MECTA-B	Noise			Blur				Weather				Digital					
Alg.	$\beta = 0.1$	auto β	Gauss.	Shot.	Impul.	Defoc.	Glass.	Motion	Zoom.	Snow	Frost	Fog	Bright.	Contr.	Elast.	Pixel.	JPEG	Orig.	Avg
EATA	✗	✗	44.4	47.1	45.4	39.0	39.4	47.4	49.7	49.7	48.4	57.6	64.3	47.8	54.5	61.7	56.3	69.5	51.4
	✓	✗	50.4	53.1	51.9	45.2	45.9	53.9	56.3	55.6	54.2	63.1	69.6	53.2	60.5	67.2	62.0	74.0	57.3
	✓	✓	**51.7**	**54.8**	**53.6**	**46.0**	**47.5**	**54.9**	**57.7**	**56.9**	**55.3**	**64.2**	**70.5**	**54.2**	**61.6**	**68.1**	**63.3**	**74.9**	**58.4**

Table 4: Evaluation of k-new K-old shift accuracy by EATA. Average accuracy (AA %) and worst accuracy (WA %) are reported for each target perturbation. Values in the brackets denote the difference between the current method and the base one. More combinations of (K, k) are in Table 8.

K	k	EMA	MECTA-B	Impul.		Motion		Fog		Elast.	
		$\beta = 0.1$	Auto β	AA	WA	AA	WA	AA	WA	AA	WA
49	1	✗	✗	35.5	34.6	37.0	36.8	50.1	49.8	48.3	47.8
		✓	✗	35.4 (**-0.1**)	30.6 (-4.0)	26.6 (-11.0)	20.1 (-16.7)	41.0 (-9.1)	25.9 (-23.9)	42.8 (**-5.5**)	39.3 (-8.5)
		✓	✓	34.4 (-1.1)	32.0 (**-2.6**)	28.6 (**-8.4**)	25.7 (**-11.1**)	43.6 (**-6.5**)	39.1 (**-10.7**)	42.6 (-5.7)	41.2 (**-6.6**)

adaptation process. Though this meanwhile decreases the accuracy, the accuracy is still higher than the BN adaptation by more than 4% based on the same batch size.

(C) Channel pruning. Fig. 2c shows that the pruning linearly reduces the maximal cache size, which bounds the maximal memory requirement in the whole adaptation life-cycle. With such a reduction in memory, pruning only mildly sacrifices the accuracy by less than 1%.

(B) Adaptive forgetting. In Fig. 2a, we observe that small batch size (corresponding to small cache size) hurts the accuracy of EATA significantly. Thus, it is crucial to ask *how the proposed adaptive forgetting and memorization improve CTA accuracy in small batches.* To answer this question, we reiterate the two keys of CTA: accurate modeling of data distribution from stream data and stability in dynamic environments. We show that our adaptive forget gate can achieve the two goals simultaneously without hyper-parameters compared to the traditional moving average method.

(B.1) Parameter-free memorization improves the per-domain accuracy. In Table 3, we present the per-domain accuracy on the full perturbation set with batch size 16 using all perturbations. We include the exponential moving average (EMA) to show that memorizing streaming batches into a moving average can improve the accuracy of small batch sizes. Despite the effectiveness of EMA, the hyperparameter β requires extra effort or extra labeled data in tuning. In contrast, MECTA-B is parameter-free and meanwhile outperforms the EMA on all corrupted and original data.

(B.2) Forgetting improves shift stability. Regarding the advantage of adaptive forgetting in Table 3, we conjecture that the adaptive β_t estimated by MECTA-B can benefit the accuracy when the data distribution shifts from one domain to another, namely, *shift accuracy* (stability). To quantify the shift accuracy, we suppose that a model first experiences K batches from one domain (old domain), and then receives k batch from another domain (new domain). The shift accuracy is the correct ratio of model predictions on samples of the k-new batches. For example, we measure the shift accuracy by randomly sampling 49 batches from the old domain and retrieving one batch from the new domain without replacement until all data of the new domain have been evaluated. For a given kind of perturbation as a new domain, we evaluate the shift accuracy paired with all kinds of perturbation as the old domain and report the *average-case accuracy* (AA) and the *worst-case accuracy* (WA). Here, we use ResNet50 on ImageNet and a *subset of perturbations* for the ease of intensive evaluations: Impul, Motion, Fog, and Elast. As summarized in Table 4, EMA causes large accuracy declines, compared to the batch-estimated BN statistics (without distribution memory). This observation implies that in contrast to the large gains in continual evaluation, the distribution memory induced by EMA becomes an obstacle for models to efficiently adapt new domains. Instead, short-term memory is preferred. Without explicitly switching a hyper-parameter, our method automatically detects such domain shift and merits the accuracy on shift with memory from past domains.

6 Conclusion

Though the gradient-based Continual Test-time Adaptation (CTA) is an effective manner to improve running performance on test data, the high memory consumption becomes a considerable challenge for deploying the technique to resource-limited end devices, like smartphones. To our best knowledge, our work is the pilot study on the memory efficiency and reveal the main bottleneck is on the intermediate results cached for back-propagation, even if only few parameters need to be updated in the state-of-the-art computation-efficient solution (EATA). Therefore, we propose the first cache-aware method that achieves higher accuracy with much lower cache memory.

ETHICS STATEMENT

In this paper, we work is not related to human subjects, practices to dataset releases, discrimination/biases/fairness concerns, adn also do not have legal compliance or research integrity issues. Our work is proposed to address the memory efficiency of model adaptation in continual distributional shifts. In this case, if the model is trained out of good will, we have good faith that our methods won't cause any ethic problem or negative social impacts.

REPRODUCIBILITY STATEMENT

The algorithm pseudo codes are enclosed in the main body. We also provide details on the implementation, hyper-parameters in Appendix B.1. The datasets and baselines codes are all public available online and we specify them properly in our paper.

ACKNOWLEDGMENTS

This research was funded by Sony AI. This material is based in part upon work supported by the National Science Foundation under Grant IIS-2212174, IIS-1749940, ECCS-2024270, Office of Naval Research N00014-20-1-2382, and National Institute on Aging (NIA) RF1AG072449.

REFERENCES

Berkin Akin, Zeshan A. Chishti, and Alaa R. Alameldeen. Zcomp: Reducing dnn cross-layer memory footprint using vector extensions. In *Proceedings of the 52nd Annual IEEE/ACM International Symposium on Microarchitecture*, pp. 126–138, Columbus OH USA, October 2019. ACM.

Arsenii Ashukha, Alexander Lyzhov, Dmitry Molchanov, and Dmitry Vetrov. Pitfalls of in-domain uncertainty estimation and ensembling in deep learning. In *International Conference on Learning Representations*, July 2021.

Han Cai, Chuang Gan, Ligeng Zhu, and Song Han. Tinytl: Reduce memory, not parameters for efficient on-device learning. *Advances in Neural Information Processing Systems*, 33:11285–11297, 2020.

Tianqi Chen, Bing Xu, Chiyuan Zhang, and Carlos Guestrin. Training deep nets with sublinear memory cost, April 2016.

Vitaliy Chiley, Ilya Sharapov, Atli Kosson, Urs Koster, Ryan Reece, Sofia Samaniego de la Fuente, Vishal Subbiah, and Michael James. Online normalization for training neural networks. In *Advances in Neural Information Processing Systems*, volume 32. Curran Associates, Inc., 2019.

Francesco Croce, Maksym Andriushchenko, Vikash Sehwag, Edoardo Debenedetti, Nicolas Flammarion, Mung Chiang, Prateek Mittal, and Matthias Hein. Robustbench: a standardized adversarial robustness benchmark, October 2021.

Jia Deng, Wei Dong, Richard Socher, Li-Jia Li, Kai Li, and Li Fei-Fei. Imagenet: A large-scale hierarchical image database. In *2009 IEEE Conference on Computer Vision and Pattern Recognition*, pp. 248–255, June 2009.

Yuyang Deng, Nidham Gazagnadou, Junyuan Hong, Mehrdad Mahdavi, and Lingjuan Lyu. On the hardness of robustness transfer: A perspective from rademacher complexity over symmetric difference hypothesis space. 2023.

Jiahua Dong, Lixu Wang, Zhen Fang, Gan Sun, Shichao Xu, Xiao Wang, and Qi Zhu. Federated class-incremental learning. In *Proceedings of the IEEE/CVF Conference on Computer Vision and Pattern Recognition*, pp. 10164–10173, 2022.

Rahul Garg and Rohit Khandekar. Gradient descent with sparsification: an iterative algorithm for sparse recovery with restricted isometry property. In *Proceedings of the 26th Annual International Conference on Machine Learning*, June 2009.

Marta Garnelo, Dan Rosenbaum, Christopher Maddison, Tiago Ramalho, David Saxton, Murray Shanahan, Yee Whye Teh, Danilo Rezende, and SM Ali Eslami. Conditional neural processes. In *International conference on machine learning*, pp. 1704–1713. PMLR, 2018.

Sachin Goyal, Mingjie Sun, Aditi Raghunathan, and Zico Kolter. Test-time adaptation via conjugate pseudo-labels. July 2022.

Kaiming He, Xiangyu Zhang, Shaoqing Ren, and Jian Sun. Deep residual learning for image recognition. *Computer Vision and Pattern Recognition*, 2016.

Dan Hendrycks and Thomas Dietterich. Benchmarking neural network robustness to common corruptions and perturbations. In *International Conference on Learning Representations*, March 2019.

Dan Hendrycks, Steven Basart, Norman Mu, Saurav Kadavath, Frank Wang, Evan Dorundo, Rahul Desai, Tyler Zhu, Samyak Parajuli, Mike Guo, Dawn Song, Jacob Steinhardt, and Justin Gilmer. The many faces of robustness: A critical analysis of out-of-distribution generalization. June 2020a.

Dan Hendrycks, Norman Mu, Ekin D. Cubuk, Barret Zoph, Justin Gilmer, and Balaji Lakshminarayanan. Augmix: A simple data processing method to improve robustness and uncertainty. In *International Conference on Learning Representations*, February 2020b.

Andrew G. Howard, Menglong Zhu, Bo Chen, Dmitry Kalenichenko, Weijun Wang, Tobias Weyand, Marco Andreetto, and Hartwig Adam. Mobilenets: Efficient convolutional neural networks for mobile vision applications, April 2017.

Gao Huang, Zhuang Liu, Laurens van der Maaten, and Kilian Q. Weinberger. Densely connected convolutional networks, January 2018.

Andrey Ignatov, Radu Timofte, William Chou, Ke Wang, Max Wu, Tim Hartley, and Luc Van Gool. Ai benchmark: Running deep neural networks on android smartphones. In *Proceedings of the European Conference on Computer Vision (ECCV) Workshops*, pp. 0–0, 2018.

Sergey Ioffe and Christian Szegedy. Batch normalization: Accelerating deep network training by reducing internal covariate shift. *arXiv:1502.03167 [cs]*, March 2015.

Yusuke Iwasawa and Yutaka Matsuo. Test-time classifier adjustment module for model-agnostic domain generalization. In *Advances in Neural Information Processing Systems*, volume 34, pp. 2427–2440. Curran Associates, Inc., 2021.

Ziyu Jiang, Xuxi Chen, Xueqin Huang, Xianzhi Du, Denny Zhou, and Zhangyang Wang. Back razor: Memory-efficient transfer learning by self-sparsified backpropagation. In *Advances in Neural Information Processing Systems*, 2022.

Ansh Khurana, Sujoy Paul, Piyush Rai, Soma Biswas, and Gaurav Aggarwal. Sita: Single image test-time adaptation, September 2022.

Pang Wei Koh, Shiori Sagawa, Henrik Marklund, Sang Michael Xie, Marvin Zhang, Akshay Balsubramani, Weihua Hu, Michihiro Yasunaga, Richard Lanas Phillips, Irena Gao, Tony Lee, Etienne David, Ian Stavness, Wei Guo, Berton Earnshaw, Imran Haque, Sara M. Beery, Jure Leskovec, Anshul Kundaje, Emma Pierson, Sergey Levine, Chelsea Finn, and Percy Liang. Wilds: A benchmark of in-the-wild distribution shifts. In *Proceedings of the 38th International Conference on Machine Learning*, pp. 5637–5664. PMLR, July 2021.

Alex Krizhevsky. Learning multiple layers of features from tiny images. Technical report, 2009.

Yanghao Li, Naiyan Wang, Jianping Shi, Jiaying Liu, and Xiaodi Hou. Revisiting batch normalization for practical domain adaptation. In *International Conference on Learning Representations*. arXiv, 2017.

Qianli Liao, Kenji Kawaguchi, and Tomaso Poggio. Streaming normalization: Towards simpler and more biologically-plausible normalizations for online and recurrent learning, October 2016.

Chenxi Liu, Lixu Wang, Lingjuan Lyu, Chen Sun, Xiao Wang, and Qi Zhu. Deja vu: Continual model generalization for unseen domains. In *International Conference on Learning Representations*, 2023.

Yuejiang Liu, Parth Kothari, Bastien van Delft, Baptiste Bellot-Gurlet, Taylor Mordan, and Alexandre Alahi. Ttt++: When does self-supervised test-time training fail or thrive? In *Advances in Neural Information Processing Systems*, volume 34, pp. 21808–21820. Curran Associates, Inc., 2021.

Arun Mallya and Svetlana Lazebnik. Packnet: Adding multiple tasks to a single network by iterative pruning. In *Proceedings of the IEEE Conference on Computer Vision and Pattern Recognition*, pp. 7765–7773, 2018.

Arun Mallya, Dillon Davis, and Svetlana Lazebnik. Piggyback: Adapting a single network to multiple tasks by learning to mask weights. In *European Conference on Computer Vision*, volume 11208, pp. 72–88, Cham, 2018. Springer International Publishing.

Zachary Nado, Shreyas Padhy, D. Sculley, Alexander D'Amour, Balaji Lakshminarayanan, and Jasper Snoek. Evaluating prediction-time batch normalization for robustness under covariate shift. *arXiv:2006.10963 [cs, stat]*, January 2021.

Shuaicheng Niu, Jiaxiang Wu, Yifan Zhang, Yaofo Chen, Shijian Zheng, Peilin Zhao, and Mingkui Tan. Efficient test-time model adaptation without forgetting. In *International Conference on Machine Learning*, 2022.

Shiori Sagawa, Pang Wei Koh, Tatsunori B. Hashimoto, and Percy Liang. Distributionally robust neural networks for group shifts: On the importance of regularization for worst-case generalization. In *ICLR*, April 2020.

Steffen Schneider, Evgenia Rusak, Luisa Eck, Oliver Bringmann, Wieland Brendel, and Matthias Bethge. Improving robustness against common corruptions by covariate shift adaptation. In *Advances in Neural Information Processing Systems*, October 2020.

Vikash Sehwag, Shiqi Wang, Prateek Mittal, and Suman Jana. Hydra: Pruning adversarially robust neural networks. In *Advances in Neural Information Processing Systems*, volume 33, pp. 19655–19666. Curran Associates, Inc., 2020.

Karen Simonyan and Andrew Zisserman. Very deep convolutional networks for large-scale image recognition, April 2015.

Yu Sun, Xiaolong Wang, Zhuang Liu, John Miller, Alexei Efros, and Moritz Hardt. Test-time training with self-supervision for generalization under distribution shifts. In *International conference on machine learning*, pp. 9229–9248. PMLR, 2020.

Mingxing Tan and Quoc V. Le. Efficientnetv2: Smaller models and faster training, June 2021.

Dequan Wang, Evan Shelhamer, Shaoteng Liu, Bruno Olshausen, and Trevor Darrell. Tent: Fully test-time adaptation by entropy minimization. In *International Conference on Learning Representations*, 2021.

Qin Wang, Olga Fink, Luc Van Gool, and Dengxin Dai. Continual test-time domain adaptation. In *Proceedings of the IEEE/CVF conference on computer vision and pattern recognition*, pp. 7201–7211, 2022a.

Zifeng Wang, Zheng Zhan, Yifan Gong, Geng Yuan, Wei Niu, Tong Jian, Bin Ren, Stratis Ioannidis, Yanzhi Wang, and Jennifer Dy. Sparcl: Sparse continual learning on the edge. In *Advances in Neural Information Processing Systems*, September 2022b.

Stephen J. Wright. Coordinate descent algorithms. *Mathematical Programming*, 151(1):3–34, June 2015.

Saining Xie, Ross Girshick, Piotr Dollár, Zhuowen Tu, and Kaiming He. Aggregated residual transformations for deep neural networks, April 2017.

Tao Yang, Shenglong Zhou, Yuwang Wang, Yan Lu, and Nanning Zheng. Test-time batch normalization, May 2022.

Geng Yuan, Xiaolong Ma, Wei Niu, Zhengang Li, Zhenglun Kong, Ning Liu, Yifan Gong, Zheng Zhan, Chaoyang He, Qing Jin, Siyue Wang, Minghai Qin, Bin Ren, Yanzhi Wang, Sijia Liu, and Xue Lin. Mest: Accurate and fast memory-economic sparse training framework on the edge. In *Advances in Neural Information Processing Systems*, volume 34, pp. 20838–20850. Curran Associates, Inc., 2021.

Sergey Zagoruyko and Nikos Komodakis. Wide residual networks. *arXiv:1605.07146 [cs]*, June 2017.

Marvin Zhang, Henrik Marklund, Nikita Dhawan, Abhishek Gupta, Sergey Levine, and Chelsea Finn. Adaptive risk minimization: Learning to adapt to domain shift. In *Advances in Neural Information Processing Systems*, December 2021.

Marvin Zhang, Sergey Levine, and Chelsea Finn. Memo: Test time robustness via adaptation and augmentation. In *NeurIPS 2021 Workshop DistShift*, January 2022.

A DISCUSSION

A.1 MEMORY FOOTPRINT FOR TEST-TIME ADAPTATION

When a learning algorithm looks for deployment on edge devices, it is unavoidable to take the two folds into account: (1) whether the maximal memory consumption of the algorithm can be fitted into a mobile device; (2) whether the dynamic and instantly-free space of device memory (RAM) is sufficient for the adaptation. The current mobile devices generally have memory in GB levels. For example, current general mobile devices such as Samsung S20 have 2GB or more memory, Raspberry Pi has 1GB or more memory. However, unlike the training or adaptation on a high-capacity GPU server where all the resources (memory and CPU time) can be allocated for training, the memory on mobile devices may be temporarily and partially allocated for the operating system and other background applications. The situation could be even more severe for mobile devices. Thus, squeezing the memory footprint dynamically is crucial for edge devices.

To avoid losing focus of the paper, we only consider the cache for gradient computation on batch-normalization layers, which has been a substantially-larger memory footprint compared to those of the widely-studied model and gradient memory in the literature (Yuan et al., 2021; Akin et al., 2019; Wang et al., 2022b). Admittedly, our work does not cover all memory consumption in the life-span of model adaptation. In Table 1, we only compute the memory costs (cache) of the back-propagation but not the forward operations, because the memory costs of the latter will be released immediately. The actual memory occupation in hardware, like NVIDIA GPU, will be enlarged due to the reservation for faster inference. The holistic solution that jointly optimizes the inference time and memory requires extra efforts on low-level computation and could be hardware-dependent. Thus, we leave the solution as a open problem for future study.

B EXPERIMENTAL DETAILS AND SUPPLEMENTARY

B.1 IMPLEMENTATION DETAILS

Hyper-parameters. All test-time adaptation objectives are optimized by stochastic gradient descent (SGD) with a momentum of 0.9. Tent and EATA utilize a batch size of 64 with a learning rate of 0.005 (0.00025) for CIFAR-10 (CIFAR100 and ImageNet). In our implementation, we use 0.0025 (0.0001) as learning rates to stabilize the training with smaller batch sizes. EATA uses 2,000 samples to estimate a Fisher matrix for anti-forgetting regularization. For MECTA, we set the threshold β_{th} for stopping layer training as 0.005 for CIFAR10/100 and 0.00125 for ImageNet-C. The cache pruning rate is set to be 0.7 for all datasets.

We implement our algorithm using PyTorch 1.12.1, cudatoolkit 11.6 on NVIDIA Tesla T4 GPUs. The codes of baselines are provided by the open sourced codes of EATA[1]. For gradient checkpointing, we use the official implementation from PyTorch, `torch.utils.checkpoint`. For each stage in the ResNet with m blocks, we will split the blocks sequentially into $\lfloor m/2 \rfloor$ segments. Therefore, ResNet50 will be split into 7 segments, approximatedly equal to $\sqrt{50}$.

Measuring cache sizes. Without GC, we measure the cache size by summing up the tensor size of all features z^l in a network. With GC, we estimate the cache size as two parts: one is the segment cache sizes and the other is the maximal cache for backwarding inside a segment. For a fair comparison, we ignore the BN's in shortcut layers (or downsample layers) in variants of ResNet, which cause a non-sequntial dependence between layers and make it hard to compute the actual cache sizes.

Measuring full footprint. In Fig. 1, we track the tensors that are cached in the GPU memory using the public tool[2]. The memory tracker will find all the PyThorch tensor variables in the garbage collector of Python. We also leverage tool, `torch.cuda.memory_cached`, provided by PyTorch to estimate the maximal GPU memory costs including non-tensor variables.

[1] https://github.com/mr-eggplant/EATA
[2] https://github.com/Oldpan/Pytorch-Memory-Utils

Implementation of stochastic cache. During forward, we will only store the remained values of z^l and the indexes of the remained channels (denoted as R). Later, we compute the gradient by

$$\sum_{n=1}^{B} \frac{\partial \ell_n}{\partial \gamma_i^l} = \begin{cases} \sum_{n=1}^{B} \sum_{j=1}^{W} \sum_{k=1}^{H} \frac{\partial \ell_n}{\partial a_{i,j,k}^l} z_{n,i,j,k}^l, & i \in R, \\ 0, & i \notin R. \end{cases}$$

As the zero values do not need cache, the implementation can effectively reduce memory consumption with a small extra space for storing the index set R.

B.2 More experimental results

MECTA in different network architectures. It is known that larger and deeper models will merit the robustness of neural networks (Hendrycks et al., 2020a). In Fig. 4, we compare the EATA and EATA+MECTA on varying model depths. We adopt the protocol in Table 2 but reduce the batch size to 32 to accommodate the huge memory cost of deeper networks. The experiments are conducted with 4 perturbations. By increasing the depth of ResNet, the cache size increases steeply. Instead, MECTA reduces the cache consumption to a low level and achieves even better accuracy. Beyond ResNet, we evaluate more network architectures in Table 5. For example, MobileNet (Howard et al., 2017) is designed for edge devices with limited computation resources. Since our method only modify the batch-normalization layers, it can be easily plugged into these networks. Except wide ResNet (WRN), our method outperforms EATA with much lower cache sizes and higher accuracy.

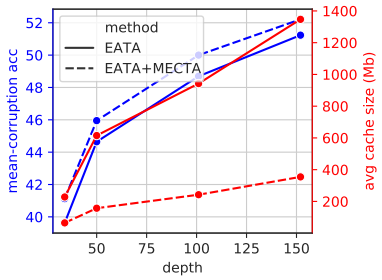

Figure 4: Evaluation on different ResNet models with varying depth.

Table 5: Evaluation on different model architectures retrived from PyTorch pre-trained models.

Architecture	Alg.	Acc. (%) Avg	Cache (Mb) Avg	Cache (Mb) Max
MobileNetV2 (Howard et al., 2017)	EATA	26.8	854.8	854.8
	EATA+MECTA	**28.0**	**233.5**	**250.5**
MobileNetV3 (Howard et al., 2017)	EATA	30.8	563.2	563.2
	EATA+MECTA	**32.2**	**158.1**	**163.7**
VGG19+BN (Simonyan & Zisserman, 2015)	EATA	34.9	1901.1	1901.1
	EATA+MECTA	**35.7**	**544.8**	**564.9**
WRN101×2 (Zagoruyko & Komodakis, 2017)	EATA	**54.7**	2716.7	2716.7
	EATA+MECTA	53.2	**803.2**	**810.4**
ResNet101	EATA	41.2	1885.0	1885.0
	EATA+MECTA	**51.3**	**449.1**	**569.8**
ResNet152	EATA	44.0	2694.3	2694.3
	EATA+MECTA	**52.9**	**635.6**	**813.6**
ResNeXt101 32×8d (Xie et al., 2017)	EATA	53.9	3802.1	3802.1
	EATA+MECTA	**54.5**	**1094.7**	**1136.1**
DenseNet121 (Huang et al., 2018)	EATA	**45.9**	2005.4	2005.4
	EATA+MECTA	42.2	**594.3**	**597.6**
EfficientNetV2-S (Tan & Le, 2021)	EATA	45.9	1556.3	1556.3
	EATA+MECTA	**47.1**	**454.4**	**463.3**

Does layer-sparse training help? In Fig. 5, we evaluate EATA with fewer trainable layers, which can reduce the cache size, following the protocol in Table 2. During adaptation, we keep k deepest layers to be trained and freeze other layers, which is denoted as Lk in the figure. We also include the EATA+GC where we use gradient checkpointing for the trainable layers. We observe that reducing the trainable layers can significantly decrease the cache size which is even lower than MECTA. However, the corresponding accuracy is significantly decreased by 5% compared to EATA+MECTA meanwhile. In comparison, though MECTA also uses the layer-sparse training, our method presents the best accuracy-memory trade-off in the experiment. The key difference is that our method sparsifies the training only on demand, specifically when a layer is well adapted without need for further training.

Does MECTA works on even smaller batches? In Table 6, we extend Table 1 with more batch sizes. One interesting observation is that our method outperforms or is comparable to other baselines given even smaller caches. For example, given a batch size of 16, EATA+MECTA can outperforms BN at the best batch size, when MECTA reduces the cache size to 71 Mb on average compared to the 134 Mb by BN.

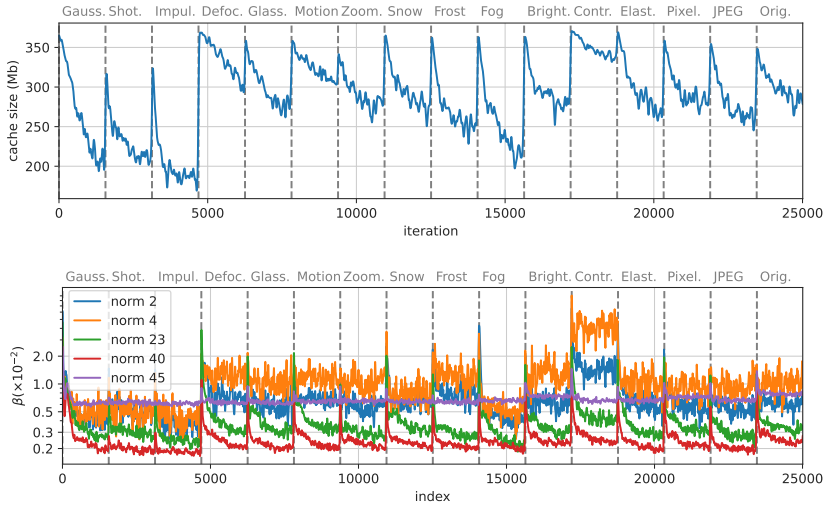

Figure 6: Dynamic cache size and β using MECTA on ImageNet-C.

Does MECTA-B works with BN adaptation and Tent? We show that MECTA-B can generally works well with BN adaptation and Tent, in Table 7. Consistent on all three backbone methods, the MECTA-B can outperforms EMA and base methods without extra hyper-parameters. EMA and MECTA-B can salvage BN and Tent from pooer performance using small batch sizes.

How does MECTA mitigate forgetting? Comparing the Tent+MECTA-B results with Tent+MECTA with 16-sized batches in Table 6, we notice that MECTA is more effective than MECTA-B on improving Tent. Thus, we conclude that the pruning and adaptive training is essential for the anti-forgetting.

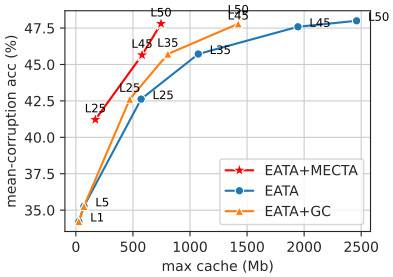

Figure 5: Compare MECTA to layer-sparse training using ResNet50 and batch size of 64. L1 means that only the deepest 1 layer is trained. Likewise, L45 denotes the deepest 45 layers.

More shift-accuracy evaluation. We consider more cases of (K, k) pairs in Table 8. In all three trials, MECTA-B reduce the shift-accuracy drops w.r.t. the baseline. Given more new-domain samples, e.g., $k = 5$, the shift-accuracy using EMA and MECTA-B becomes higher than the baseline, implying the quick convergence of the adaptation.

Cache size and β by iteration. We extend Fig. 3 to a full life-cycle version in Fig. 6. For evaluating β, we run the experiment on ImageNet-C using ResNet50 and we use MECTA with EATA for adaptation. In more corruptions, we find the periodic fluctuation of β by the distributional shifts, which results in the dynamic cache sizes.

Table 6: Continual evaluation on three datasets with the highest severity level 5 regarding accuracy (%). For a fair comparison, batch sizes (BS) are chosen such that the corresponding cache sizes are lower than those of BN with batch size of 128. Blue cells highlight the accuracy that is the highest among all methods, and the bold texts indicate the best accuracy given the same base algorithm.

		Noise			Blur				Weather				Digital					Acc.	Cache	
Alg.	BS	Gauss.	Shot.	Impul.	Defoc.	Glass.	Motion	Zoom.	Snow	Frost	Fog	Bright.	Contr.	Elast.	Pixel.	JPEG	Orig.	Avg	Avg	Max
CIFAR10-C																				
BN	32	80.2	82.0	78.7	91.2	79.2	89.9	91.0	86.9	86.6	84.5	91.9	88.8	84.2	86.8	81.8	93.2	86.1	34	34
BN	64	81.3	82.7	79.6	91.9	79.9	90.8	91.6	87.5	87.0	85.5	92.3	89.4	85.3	87.5	82.6	93.7	86.8	67	67
BN	128	**81.5**	**83.2**	**79.9**	**92.4**	**80.7**	**91.1**	**92.1**	**87.9**	**87.7**	**85.7**	**92.7**	**89.8**	**85.6**	**87.6**	**83.0**	**94.2**	**87.2**	134	134
Tent	8	68.8	46.3	16.4	12.8	11.8	8.9	9.9	10.7	10.3	10.2	10.3	10.2	10.1	10.0	10.2	10.2	16.7	100	100
	16	81.8	82.2	71.8	68.9	52.8	43.7	39.0	30.7	22.8	17.7	10.1	6.7	7.4	8.2	8.1	9.0	35.1	199	199
	32	86.0	87.5	84.1	88.8	81.2	85.5	86.6	85.5	86.6	83.5	88.5	87.0	83.0	85.7	80.7	87.2	85.5	398	398
+MECTA	16	86.7	88.3	85.1	90.0	79.9	85.7	88.2	85.4	86.4	83.5	88.7	88.0	83.0	86.2	79.6	86.2	85.7	41	60
+MECTA	32	**87.0**	**88.6**	**85.7**	**91.8**	**84.5**	**90.9**	**92.5**	**90.1**	**91.3**	**88.8**	**93.2**	**92.0**	**88.0**	**90.5**	**86.0**	**93.8**	**89.7**	62	119
EATA	8	74.5	70.9	66.6	69.7	55.5	54.6	47.2	38.4	33.1	35.1	35.2	18.8	12.2	14.5	13.3	8.5	40.5	100	100
	16	83.4	84.3	81.3	86.4	77.0	83.8	86.5	84.5	84.7	83.9	88.1	87.9	80.9	85.5	79.3	87.9	84.1	199	199
	32	85.7	87.6	85.7	89.8	82.5	88.3	90.0	88.2	88.8	88.7	91.4	91.0	85.5	89.5	85.3	90.6	88.0	398	398
+MECTA	16	86.5	88.2	84.6	89.8	83.0	88.5	90.4	88.4	88.9	88.8	91.7	91.1	85.8	89.5	85.3	92.3	88.3	45	60
+MECTA	32	**87.1**	**89.3**	**86.8**	**92.0**	**85.6**	**90.7**	**92.3**	**90.8**	**91.1**	**89.7**	**93.3**	**92.5**	**88.0**	**91.0**	**86.9**	**93.5**	**90.0**	71	119
CIFAR100-C																				
BN	32	56.2	57.1	54.7	70.5	56.3	68.6	70.2	63.0	63.5	56.6	71.9	68.0	62.2	64.8	56.7	73.8	63.4	34	34
BN	64	56.8	58.7	55.8	71.5	57.7	69.5	71.5	64.1	64.3	57.4	73.1	69.0	63.6	66.1	58.4	75.3	64.6	67	67
BN	128	**57.6**	**59.0**	**56.6**	**72.5**	**58.2**	**69.9**	**71.8**	**64.7**	**64.8**	**57.9**	**73.5**	**69.8**	**64.3**	**66.7**	**58.6**	**75.8**	**65.1**	134	134
Tent	8	52.9	53.9	46.7	50.5	31.2	29.7	23.7	14.3	10.0	6.7	5.9	3.4	3.9	3.6	3.5	3.5	21.5	100	100
	16	56.8	61.4	59.6	68.5	56.1	65.3	66.9	59.7	60.0	54.9	65.0	57.0	54.2	56.2	46.8	58.6	59.2	199	199
	32	58.5	**63.0**	**61.6**	71.8	60.3	69.7	71.8	65.1	66.3	60.9	72.4	68.7	64.7	67.8	59.7	74.3	66.0	398	398
+MECTA	16	58.4	**63.0**	**61.1**	73.3	60.7	71.3	73.4	66.2	66.4	61.0	73.5	67.7	65.5	68.2	59.3	75.5	66.5	50	60
+MECTA	32	**58.6**	61.5	60.1	**73.9**	**61.0**	**72.4**	**74.9**	**66.8**	**68.1**	**61.9**	**75.3**	**71.3**	**66.7**	**70.5**	**61.7**	**78.1**	**67.7**	77	120
EATA	8	52.1	54.2	53.2	65.3	51.5	63.8	64.9	59.1	58.5	53.9	66.8	63.2	56.3	61.1	52.9	70.1	59.2	100	100
	16	57.3	60.5	58.5	69.9	57.1	68.9	69.8	63.7	64.4	59.4	71.6	67.9	62.8	67.1	58.2	74.4	64.5	199	199
	32	58.4	**62.4**	**60.9**	72.1	59.5	70.3	72.4	66.3	66.5	**62.2**	74.4	70.8	65.3	69.4	61.0	76.9	66.8	398	398
+MECTA	16	58.4	61.5	59.3	**73.2**	59.8	**71.6**	73.1	**66.9**	66.9	60.8	74.4	70.9	65.0	68.8	60.6	77.2	66.8	52	60
+MECTA	32	**58.7**	**62.0**	**60.0**	73.0	**60.5**	71.3	**73.9**	66.7	**67.3**	**62.0**	**75.3**	**71.7**	**66.3**	**69.8**	**61.5**	**78.0**	**67.4**	81	120
ImageNet-C																				
BN	64	38.4	41.6	38.8	29.1	32.1	40.1	46.4	44.1	46.8	54.8	67.7	35.1	53.7	64.7	54.6	73.5	47.6	206	206
BN	128	**39.2**	**42.6**	**39.6**	**29.9**	**32.9**	**40.8**	**47.4**	**45.0**	**47.7**	**55.8**	**68.5**	**36.0**	**54.8**	**65.4**	**55.7**	**74.2**	**48.5**	411	411
Tent	8	33.8	16.5	0.8	0.4	0.3	0.4	0.4	0.4	0.4	0.3	0.4	0.2	0.3	0.4	0.3	0.4	3.5	307	307
	16	43.3	46.1	42.8	25.8	14.8	5.0	1.3	0.7	0.7	0.7	0.8	0.6	0.7	0.7	0.7	0.7	11.6	615	615
	32	46.1	50.6	49.2	37.2	38.2	41.2	42.5	36.6	36.2	38.8	46.8	27.5	30.5	34.3	26.9	34.8	38.6	1230	1230
+MECTA	16	**48.0**	**52.9**	**51.8**	**38.9**	42.0	46.5	49.5	44.0	43.9	47.7	56.6	38.3	44.1	49.5	43.2	52.7	46.8	158	187
+MECTA	32	47.0	52.3	51.7	38.5	**43.1**	**47.5**	**51.5**	**47.4**	**49.3**	**54.2**	**64.4**	**46.2**	**55.6**	**62.4**	**57.0**	**68.8**	**52.3**	269	373
EATA	8	34.1	37.0	35.0	27.5	28.1	35.5	38.6	39.6	39.7	47.8	56.6	35.5	44.1	53.3	46.7	63.2	41.4	307	307
	16	44.4	47.1	45.4	39.0	39.4	47.4	49.7	49.7	48.4	57.6	64.3	47.8	54.5	61.7	56.3	69.5	51.4	615	615
	32	49.0	52.3	51.1	44.4	45.2	52.3	55.1	54.0	52.7	61.3	67.6	52.7	58.8	65.3	60.4	72.3	55.9	1230	1230
+MECTA	16	48.6	51.7	49.7	42.9	44.4	51.6	55.4	54.5	53.4	62.5	70.0	51.8	60.1	67.6	61.7	**74.7**	56.3	162	187
+MECTA	32	**50.3**	**54.1**	**52.6**	**44.6**	**47.0**	**53.6**	**57.0**	**55.5**	**54.8**	**62.9**	**70.3**	**54.3**	**61.1**	**68.4**	**63.0**	74.6	**57.8**	288	373

Table 7: Ablation study of MECTA-B on ImageNet-C with the highest severity level 5 regarding accuracy (%) and a batch size of 16. Blue cells highlight the accuracy that is the highest among all methods, and the bold texts indicate the best accuracy among ablations of EMA and MECTA-B.

	EMA	MECTA-B	Noise			Blur				Weather				Digital					
Alg.	$\beta = 0.1$	auto β	Gauss.	Shot.	Impul.	Defoc.	Glass.	Motion	Zoom.	Snow	Frost	Fog	Bright.	Contr.	Elast.	Pixel.	JPEG	Orig.	Avg
BN	✗	✗	33.7	36.5	34.0	24.6	27.2	35.0	40.5	39.1	42.3	49.4	62.7	30.7	47.6	59.1	48.9	69.1	42.5
	✓	✗	36.4	40.4	36.4	28.6	31.8	40.1	47.0	43.2	46.4	53.9	67.8	32.3	53.8	64.9	55.2	74.2	47.0
	✓	✓	**37.8**	**41.9**	**37.7**	**29.3**	**32.7**	**40.6**	**47.9**	**44.0**	**47.2**	**55.0**	**68.6**	**32.9**	**55.0**	**65.8**	**55.9**	**74.8**	**47.9**
Tent	✗	✗	43.3	46.1	42.8	25.8	14.8	5.0	1.3	0.7	0.7	0.7	0.8	0.6	0.7	0.7	0.7	0.7	11.6
	✓	✗	48.5	52.6	51.0	37.8	36.4	38.6	38.3	29.7	25.8	23.0	24.9	6.1	6.6	5.3	1.6	2.3	26.8
	✓	✓	**50.0**	**53.9**	**52.2**	**38.7**	**38.3**	**40.9**	**41.3**	**33.8**	**31.4**	**30.6**	**34.8**	**12.6**	**14.5**	**13.0**	**7.0**	**9.2**	**31.4**
EATA	✗	✗	44.4	47.1	45.4	39.0	39.4	47.4	49.7	49.7	48.4	57.6	64.3	47.8	54.5	61.7	56.3	69.5	51.4
	✓	✗	50.4	53.1	51.9	45.2	45.9	53.9	56.3	55.6	54.2	63.1	69.6	53.2	60.5	67.2	62.0	74.0	57.3
	✓	✓	**51.7**	**54.8**	**53.6**	**46.0**	**47.5**	**54.9**	**57.7**	**56.9**	**55.3**	**64.2**	**70.5**	**54.2**	**61.6**	**68.1**	**63.3**	**74.9**	**58.4**

Table 8: Evaluation of k-new K-old shift accuracy by EATA. Average accuracy (AA %) and worst accuracy (WA %) are reported for each target perturbation. Values in the brackets denote the difference between the current method and the base method using batch statistics.

K	k	EMA	MECTA-B	Impul.		Motion		Fog		Elast.	
		$\beta = 0.1$	Auto β	AA	WA	AA	WA	AA	WA	AA	WA
49	1	✗	✗	35.5	34.6	37.0	36.8	50.1	49.8	48.3	47.8
		✓	✗	35.4 (**-0.1**)	30.6 (-4.0)	26.6 (-11.0)	20.1 (-16.7)	41.0 (-9.1)	25.9 (-23.9)	42.8 (**-5.5**)	39.3 (-8.5)
		✓	✓	34.4 (-1.1)	32.0 (**-2.6**)	28.6 (**-8.4**)	25.7 (**-11.1**)	43.6 (**-6.5**)	39.1 (**-10.7**)	42.6 (-5.7)	41.2 (**-6.6**)
9	1	✗	✗	34.1	33.4	35.7	35.6	49.4	48.9	47.4	47.1
		✓	✗	32.8 (-1.3)	27.0 (-6.4)	25.0 (-10.7)	17.3 (-18.3)	38.4 (-11.0)	23.9 (-25.0)	41.1 (-6.3)	35.7 (-11.4)
		✓	✓	34.1 (**0.0**)	32.3 (**-1.1**)	27.4 (**-8.3**)	23.1 (**-12.5**)	42.4 (**-7.0**)	36.5 (**-12.4**)	41.9 (**-5.5**)	40.0 (**-7.1**)
45	5	✗	✗	35.4	34.6	36.9	36.5	50.3	49.3	48.5	47.7
		✓	✗	38.4 (+3.0)	37.5 (+2.9)	35.4 (-1.5)	30.6 (-5.9)	53.3 (+3.0)	50.2 (0.9)	52.0 (+3.5)	50.8 (+3.1)
		✓	✓	37.8 (+2.4)	37.2 (+2.6)	35.4 (-1.5)	33.0 (**-3.5**)	51.5 (+1.2)	49.6 (+0.3)	50.8 (+2.3)	49.6 (+1.9)